Ultra-Sensitive Molecular Detection Using Thermal Conductance of a Hydrophobic Gold Water Interface.

ARTICLE *in* NANO LETTERS · AUGUST 2013

Impact Factor: 13.59 · DOI: 10.1021/nl401717y · Source: PubMed

4 AUTHORS, INCLUDING:

Arwa Alaulamie
Ohio University
2 PUBLICATIONS **4** CITATIONS
SEE PROFILE

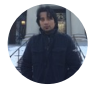

Susil Baral
Ohio University
6 PUBLICATIONS **16** CITATIONS
SEE PROFILE

Hugh Hill Richardson
Ohio University
98 PUBLICATIONS **2,132** CITATIONS
SEE PROFILE

NANO LETTERS

Letter

pubs.acs.org/NanoLett

Ultrasensitive Molecular Detection Using Thermal Conductance of a Hydrophobic Gold–Water Interface

Andrew J. Green, Arwa A. Alaulamie, Susil Baral, and Hugh H. Richardson*

Department of Chemistry and Biochemistry, Ohio University, Athens, Ohio 45701, United States

Supporting Information

ABSTRACT: The thermal conductance from a hydrophobic gold aqueous interface is measured with increasing solute concentration. A small amount of aqueous solute molecules (1 solute molecule in 550 water molecules) dramatically increases the heat dissipation into the surrounding liquid. This result is consistent with a thermal conductance that is limited by an interface interaction where minority aqueous components significantly alter the surface properties and heat transport through the interface. The increase in heat dissipation can be used to make an extremely sensitive molecular detector that can be scaled to give single molecule detection without amplification or utilizing fluorescence labels.

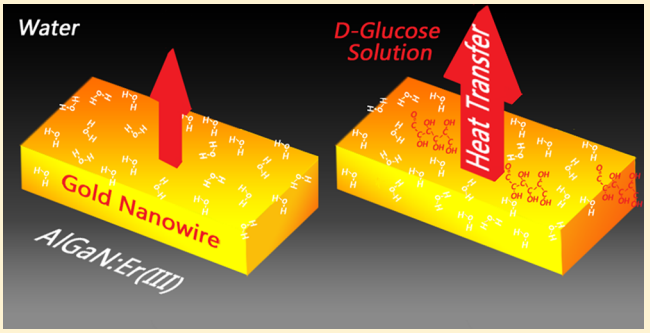

KEYWORDS: *Molecular detection, heat generation, gold nanowires, absorption cross section, thermal conductance*

Single molecule detection is essential for pharmaceutical applications where even small transcription errors lead to a large heterogeneity in molecular ensembles assumed to be identical.[1,2] Additionally, understanding heat transfer at a solid–water interface is critical to develop medical therapies where nanoscale heaters are used for photothermal therapy,[3−6] drug delivery,[7,8] water sterilization,[9] imaging,[10] and biological actuation.[11] Electrolyte adsorbates also show a significant effect on a gold nanoparticle's plasmon properties.[12,13] Many current single molecule techniques require amplification and labels to boost sensitivity to reach the single molecule level. Recently, molecule detection, approaching a single molecule, has been realized from a specially designed array of nanodots that exhibits zero reflection. This approach benefits both from plasmonic field enhancement and phase properties of reflected light to enhance sensitivity to the single molecule level.[13] Optical measurements utilizing reflection or scattering have a polarizability squared dependence while absorption measurements are proportional to polarizability.[14] Polarizability scales with the nanostructure volume and as a result, scattering measurements fall off as the volume squared while absorption measurements only decrease linearly with volume. As a result, absorption measurements have the potential to be inherently more sensitive than scattering measurements for smaller nanostructures.

The effect of chemical bonding on heat transport across a gold–quartz interface has been elucidated,[15] and remarkably, a change in a single bond at the interface affects the heat transport through the interface. This suggests that thermal transport through the interface is facilitated or impeded on length scales that are on the order of chemical bonds. Also, ligands on a gold nanorod surface immersed in water have been shown to alter the interface thermal conductance.[16] A totally different picture emerges if the region that affects thermal transport is many monolayers thick. This effect could be especially pronounced in solid–liquid interfaces where the surface properties alter the properties of interfacial water. The local density of interfacial water is affected by the wettability of a gold surface. Hydrophilic surfaces tend to have a higher water density compared to the bulk[17] while hydrophobic surface have a thin layer of low density water near the surface.[18,19] The interface thermal conductance depends upon how well water adheres to a surface,[15,19−21] and the adhesion energy of water on gold surfaces can be tuned with self-assembled monolayers (SAMs) with different end groups. Hydrophilic surfaces facilitate heat flow into the surroundings while hydrophobic surfaces impede heat dissipation to the surroundings.[21] In this paper, we show that an extremely small amount of aqueous solute molecules (1 solute molecule in 550 water molecules) increases the heat flow through a hydrophobic gold–water interface. This result is consistent with an extremely localized interfacial interaction where minority aqueous components significantly alter the surface properties and thermal transport through the interface. We show that this property can be used to make an extremely sensitive molecular detector that is capable of single molecule detection without amplification or utilizing fluorescence labels.

Materials and Methods. *Optical Measurements of Temperature.* The optical measurements and characterization of the thermal sensor film has been described in detail

Received: May 10, 2013
Revised: June 26, 2013
Published: August 7, 2013

previously.[22] We use 532 Nd/YAG CW laser to excite a thin film (~270 nm thick) of $Al_{0.94}Ga_{0.06}N$ embedded with Er^{3+} ions on a silicon substrate. The thin film acts as a thermal sensor film by measuring the relative photoluminescent intensities of the $^2H_{11/2} \rightarrow {}^4I_{15/2}$ and the $^4S_{3/2} \rightarrow {}^4I_{15/2}$ energy transitions of the Er^{3+} ions. These intensities have been shown to be temperature dependent[23,24] and are related by a Boltzmann factor ($\exp(-\Delta E/kT)$ where ΔE is the energy difference between the two levels, k is the Boltzmann constant, and T is the absolute temperature. The optical temperature measurements were made with a WITec α-SNOM300s. The same Nd:YAG laser with adjustable power is focused with a 50× objective (Zeiss EC-Epiplan-NEOFLUAR 50X/0.8 HD) onto the thin film thermal sensor. If the data is collected with the sample submerged in water, a Nikon 60× water immersion lens is used. The emitted light from the thermal sensor is collected with the same objective and sent to the CCD spectrograph with a collection fiber. The laser will simultaneously excite both the thermal sensing thin film and the gold nanowire. The nanostructures can be seen using bright-field microscopy, once found, the thermal sensor film is translated with nanometer control under the objective during laser excitation. An image is collected by storing the full photoluminescence spectrum at pixel locations within the image (100 nm × 100 nm pixel size). A temperature image is constructed from the photoluminescence spectra at each pixel location. The collected spectra is smoothed using Savitzky-Golay fourth order and sacrificing 10 data points at the end of the spectrum. The scanning rate moves 100 nm every 0.03 s. The long time scales ensure the thin film temperature is in equilibrium with the nanowire. The maximum temperature measured minus the background temperature gives the change in temperature of the nanoparticle. Dynamic temperature measurements were also taken by monitoring the spectra over time. A survey spectral image was first taken to locate the particle. Spectra were then taken while focused on the particle over a period of time.

Fabrication of Gold Nanowires. The gold nanowires are fabricated using conventional e-beam lithography with lift-off. The height of the nanowires is 64 nm measured with a Nanoscope IIIA Multimode AFM. The nanowires have a standard width of 108 nm and vary in length from 470 to 1100 nm. The width and length was measured with a JEOL JSM-5300 scanning electron microscope. A single layer of around 100 nm of poly(methyl methacrylate) (PMMA) (950K A4 PMMA in Anisole) positive resist was spin coated onto the $Al_{0.94}Ga_{0.06}N/Er^{3+}$ thin film on Si. The PMMA was filtered through a 0.2 um frit to remove bubbles. The PMMA-coated samples were baked on a hot plate at 205 °C for 5 min. After baking, electron beam irradiation (~50 kV) was performed to draw the desired pattern/dots arrays with a resolution of ~10 nm. The samples were then developed with MIBK/IPA = 1:3 (volume) for 30 s and rinsed/cleaned in isopropyl alcohol (IPA) and dried with N_2. A thin adhesion layer of Ti (5 nm) was first deposited then followed by a thicker (60 nm) layer of Au using DC sputtering. The residual layer was removed with warm a (60 °C) acetone bath. All subsequent cleaning was done with a sonication bath in IPA.

Results. *Heat Generation and Temperature Change from a Single Gold Nanowire.* Figure 1 shows SEM image of the lithographically fabricated gold nanowires. The standard width and height of the nanowires is 108 and 64 nm respectively with lengths of 470, 580, 860, and 1100 nm. Three-dimensional (3D) thermal images of 470 nm long nanowire excited with 3.0 × 10^9 W/m^2 laser intensity surrounded by air, water, 2% g/g sucrose, and 2% g/g NaCl are shown in Figure 2. The maximum measured temperature decreases when the sample is submerged in water and continues to decrease with increasing solute molality. It should be noted that the solute molality of 2% g/g NaCl and 2% g/g D-glucose is 1.3 m and 0.11 m respectively. The ionization factor for sugar and NaCl is 1 and 1.9 respectively.

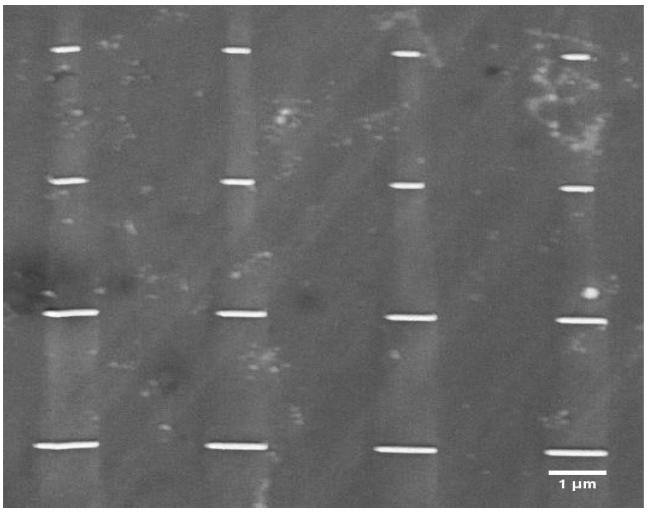

Figure 1. An SEM image of lithographically fabricated gold nanowires with a standard height and width of 64 and 108 nm, respectively. The lengths from smallest to largest are 470, 580, 860, and 1100 nm.

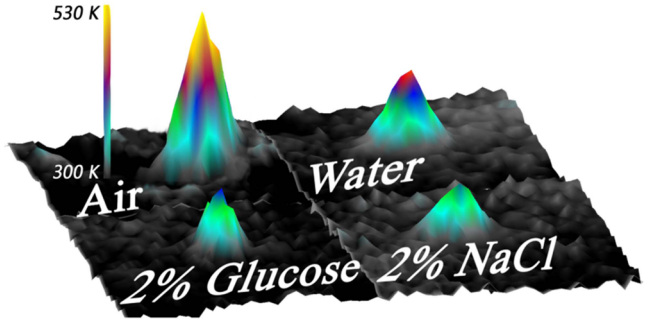

Figure 2. A 3D thermal image of the smallest gold nanowire in Figure 1 with different surroundings of air, water, 2% g/g NaCl, and 2% g/g D-glucose. The excitation intensity in every image is 3.0 × 10^9 W/m^2.

Figure 3 demonstrates the temperature change of the 470 nm nanowire as a function of laser intensity. We measured the change in temperature of the nanostructure in air, water, and varying solutions of glucose and NaCl. The heat slope decrease when the particle is submerged in water. More heat is dissipated when the sample is immersed in water compared to air and a lower steady-state temperature is observed at the same laser intensity. The substrate is immersed with five different solutions of varying solute concentration. The three solutions are 2, 3, and 4% g/g of D-glucose with two more solutions of 2 and 4% by mass NaCl. As seen in Figure 3, the heat slopes deflect further with increasing solute concentration.

Figure 4 depicts the temperature change as a function of time for a 250 nm long nanowire. A survey temperature scan was imaged to locate the nanowire on the substrate. The temperature was then monitored as a function of time with a constant laser intensity of 1.6 × 10^{10} W/m^2. The nanowire has

dx.doi.org/10.1021/nl401717y | Nano Lett. 2013, 13, 4142−4147

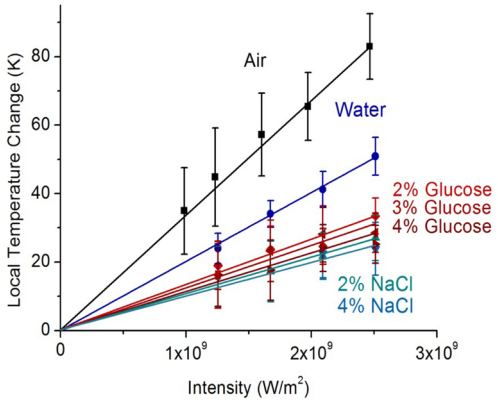

Figure 3. A plot that shows the change in temperature of the smallest gold nanowire as a function of incident laser intensity. The nanostructure temperature is measured while surrounded in air, water, 2% g/g, 3% g/g, and 4% g/g D-glucose, and 2% g/g and 4% g/g NaCl solutions.

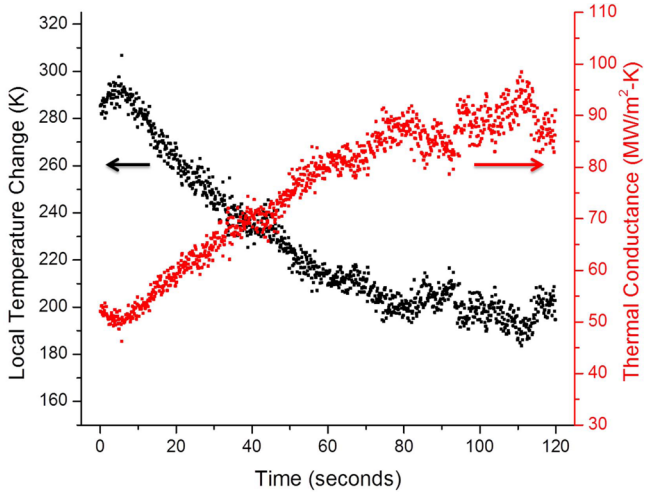

Figure 4. The temperature of a hydrophobic-coated gold nanoparticle surrounded by water is measured as a function of time (black). The decrease in temperature relates to the removal of the hydrophobic layer. This increases the heat dissipation, in turn lowering the steady-state temperature. The temperature is then transformed in the thermal conductance and is plotted in red.

a monolayer of chloroform on the surface that is displaced with water over time when heated. The local temperature change (shown as black dots) decreases with time as the heat dissipation into the surrounding liquid increases.

Discussion. *Model of Heat Transfer.* The temperature of the nanoparticle is directly related to how well heat transfers into the surroundings. The following section details our method for determining how much heat is dissipated per second from each surface of the nanostructure. The temperature profile at all points in the nanowire is the same because the thermal conductivity of the gold nanowire is much larger than the thermal conductivity of the surroundings. The nanowires become thermalized with a temperature equivalent to the temperature maximum. The maximum measured temperature change is observed when the nanowire is irradiated at the center of the nanowire. A steady-state temperature is obtained when the amount of heat generation is equal to the amount of heat dissipation. The heat generation is the product of absorption cross section and average laser intensity. The heat dissipation depends upon whether the nanowire is immersed in air or water. In air, heat only dissipates into the substrate and is given by eq 1

$$\dot{q}_{\mathrm{gen}}^{\mathrm{air}}(W) = C_{\mathrm{abs}}^{\mathrm{air}} I_{\mathrm{avg}} = \dot{q}_{\mathrm{diss}}^{\mathrm{air}} = 12.8 h_{\mathrm{sub}} \Delta T_{\mathrm{max}} \iint_{x,y} \mathrm{d}x\ \mathrm{d}y \tag{1}$$

The parameter h_{sub} is the heat transfer coefficient into the substrate and x and y are dimensions along the width and length of the nanowire, respectively. The factor 12.8 in the heat dissipation term relates the local temperature of the nanowire to the measured temperature.[22] This factor takes into account that our optical measurement of temperature is resolution limited and needs to be convoluted with the collection volume of our microscope and the true thermal image in the substrate. The thermal transfer parameter is a function of the numerical aperture of the objective used to make the measurement.[25] The temperature measurements in air and water use different objectives with numerical apertures of 0.8 and 1.0, respectively. The thermal transfer parameter relates the measured temperature (convolution of the sampled substrate temperature with the microscope point spread function) to the local temperature of the substrate at the nanowire. The thermal transfer parameter in air is 12.8 using an objective with a numerical aperture of 0.8 and a collecting fiber with an internal diameter of 25 μm.[22] When the water immersion lens is used, the thermal transfer parameter is scaled by the ratio of the numerical apertures and becomes 10.2, that is, $10.2 = (12.8 \times 0.8)/(1.0)$.The absorption cross section at 532 nm is calculated for different nanowire lengths in both air and water (see section below). Once the absorption cross section and two-dimensional temperature profile are known, then a substrate thermal transfer coefficient of 82 MW/m^2·K is determined using eq 1. This value is in reasonable agreement with gold sputtered films on SiO_2 substrates.[26] The heat dissipation per second for the nanowires immersed in water adds a new dissipative channel where heat can dissipate into water at the gold/water interface. The total heat dissipation per second when the nanowire is immersed in water is given by eq 2

$$\dot{q}_{\mathrm{diss}}^{\mathrm{water}}(W) = 10.2(h_{\mathrm{sub}} \Delta T_{\mathrm{max}} \iint_{x,y} \mathrm{d}x\ \mathrm{d}y + h_{\mathrm{water}} \Delta T_{\mathrm{max}} \iint_{x,y} \mathrm{d}x\ \mathrm{d}y + 2h_{\mathrm{water}}(\Delta T_{\mathrm{max}} \iint_{y,z} \mathrm{d}y\ \mathrm{d}z + \Delta T_{\mathrm{max}} \iint_{x,z} \mathrm{d}x\ \mathrm{d}z)) \tag{2}$$

The parameter h_{water} is the thermal transfer coefficient for heat dissipation from the gold interface into water and z is the dimension along the height of the nanowire. This model assumes that the lithographically prepared nanowire is a rectangular box having dimensions x, y, and z corresponding to the width, length, and height, respectively. At steady state, $\dot{q}_{\mathrm{gen}}^{\mathrm{water}} = C_{\mathrm{abs}}^{\mathrm{water}} I_{\mathrm{avg}} = \dot{q}_{\mathrm{diss}}^{\mathrm{water}}$, and h_{water} is determined using the calculated absorption cross section in water and assuming that the heat transfer coefficient to the substrate does not change when the sample is submerged in water.

Average Laser Intensity over the Nanowire. The laser intensity is given by a two-dimensional Gaussian profile that depends upon the full width half-maximum (fwhm) of the laser spot.[22] The laser intensity is not constant over the gold wire but

dx.doi.org/10.1021/nl401717y | Nano Lett. 2013, 13, 4142−4147

varies along the wire. I_{avg} is the average laser intensity illuminating the nanostructure. The average laser intensity is determined by first integrating the laser intensity over the two-dimensional dimensions of the nanowire and then restricting the length dimension to where half of the integrated intensity is obtained. The laser intensity at this restricted dimension is a constant and set to I_{avg}. The product of I_{avg} and C_{abs} gives the total heat generation.

Absorption Cross Section for Nanowires in Air and Water. Mie theory[14] is used to calculate the absorption cross section for the four nanowires (see Supporting Information). Briefly, a prolate spheroid shape was used to approximate the rectangular shape of the nanowire. The absorption cross section C_{abs}, is given by eq 3 where ε_{eff} is the effective dielectric constant of the surrounding medium, λ is the wavelength, and α_j is the polarizability. The polarizability is a function of the particle's size, shape, and dielectric constant. The effective dielectric constant is determined using a theoretical model for particle–substrate interactions and how these interactions influence the localized plasmon resonances of spheres and nanowires.[27]

$$C_{abs} = -8\frac{\pi^2}{\lambda}\sqrt{\varepsilon_{eff}}\ \mathrm{Im}(\alpha_j) \tag{3}$$

The nanowire is excited with the laser polarized along the nanowire axis where only the longitudinal mode is excited. The absorption cross sections for the longitudinal mode of the different nanowire lengths, in both air and water, are presented in Table 1. Figure 5 shows the calculated absorption cross section as a function of wavelength for the 470 nm (black and green) and 1100 nm (blue and red) nanowire. The region around the excitation wavelength of 532 nm has been enlarged by a factor of 10 for clarity in this region.

Table 1. The Calculated Absorption Cross Sections of the Longitudinal Mode for the Four Au Nanowires of Different Lengths[a]

NW length (nm)	σ_{abs} in air (m^2)	σ_{abs} in water (m^2)
250	2.40×10^{-13}	1.06×10^{-13}
470	1.49×10^{-13}	9.24×10^{-14}
580	1.51×10^{-13}	9.96×10^{-14}
860	1.77×10^{-13}	1.27×10^{-13}
1100	2.09×10^{-13}	1.53×10^{-13}

[a]The cross sections are calculated with the particle sitting on a substrate of AlN and surrounded by either air ($\varepsilon_b = 1$) or water ($\varepsilon_b = 1.77$). The value listed is the absorption cross section at the excitation wavelength (532 nm).

Heat Transfer Coefficient from Nanowire into Water. The transfer coefficients for heat dissipation of nanowires into aqueous solutions of different concentrations are shown in Figures 6 and 7. Figure 6 plots the thermal conductance for all the nanowires of different lengths while Figure 7 shows the thermal conductance for the 470 nm long nanowire as a function of number of adsorbed molecules. There is a slight difference between thermal conductance from nanowires of different lengths with only a slight increase with nanowire length. Pure water (zero molality) has an extremely low thermal conductance around 11 ± 7 MW/m^2·K. The thermal conductance for a hydrophobic gold–water interface has been measured to be around 50 MW/m^2·K and 100 MW/m^2·K for a hydrophilic gold–water interface.[21] Our result is surprising as a much higher heat transfer coefficient is expected.[28] An extremely low value for thermal conductance into water suggests that the gold–water interface is hydrophobic.[19,21] Wettability of electrolyte solutions above metal interfaces have been studied both experimentally and theoretically.[29−33] We believe that sonication in IPA leaves a residual hydrophobic layer on the gold resulting in the low thermal conductance. The solution specific heat, density, and viscosity change very little with solute concentration in the range of this study (4% by mass). The behavior of solvated ions with at a gold interface have been studied previously.[34,35] This implies that the solution effusivity changes little for all aqueous solutions and, consequentially, the solution heat dissipation properties should be invariant to addition of solutes to the solution. A Kapitza length of 55 nm is calculated from (Λ_f /h_{water}) where Λ_f is the thermal conductivity of water of 0.6 W/m^2·K and h_{water} is the thermal conductance of 11 MW/m^2·K. Adding solutes to the solution increased the thermal conductance from ~10 MW/m^2·K to a saturation value of 50 ± 20 MW/m^2·K. The increase in

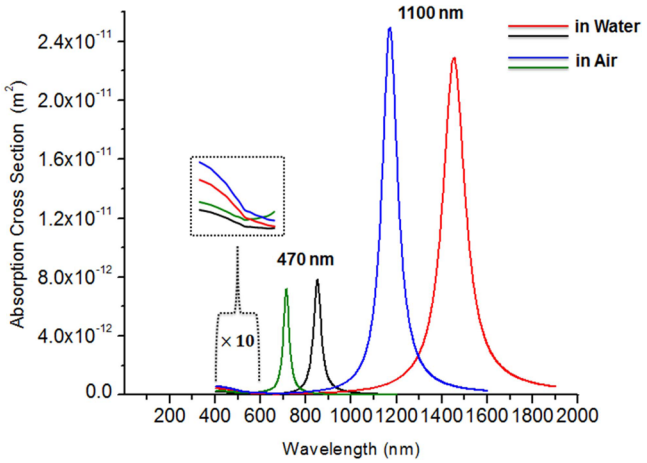

Figure 5. The absorption cross section for two gold nanowires (470 and 1100) is calculated and plotted as a function of wavelength. The absorption cross section is a function of the surrounding dielectric constants and therefore red shifts when surrounded by water. The maximum absorption wavelength also red shifts as a function of aspect ratio. The inset shows the abruption values at the excitation wavelength of 532 nm.

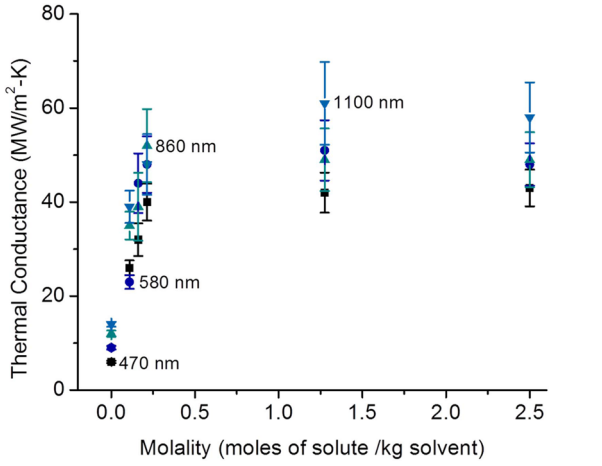

Figure 6. A plot that shows the measured thermal conductance as a function of solute concentration. The dots correspond to the 470, 580, 860, and 1100 nm wires. The thermal conductance increases rapidly with solute molality and levels off at approximately 0.3 m.

dx.doi.org/10.1021/nl401717y | Nano Lett. 2013, 13, 4142−4147

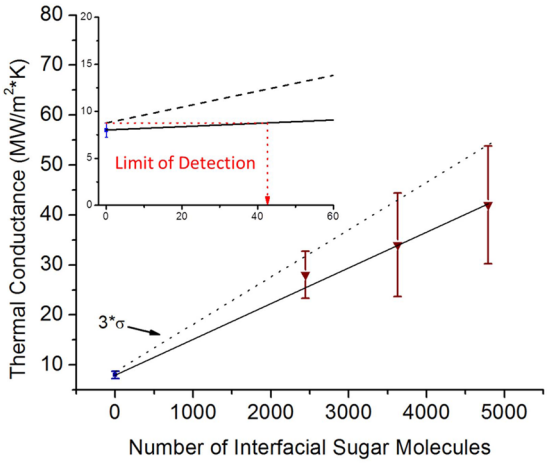

Figure 7. A plot of thermal conductance as a function of adsorbed solute molecules. The number of solute molecules adsorbed onto the surface is calculated through the concentration of the solution. The error bars in this figure are three times the standard deviation. The dotted lines show the how the standard deviation decreases with the number of molecules adsorbed. The red line shows the point at which the lower limit rises above the minimum upper limit, this is the limit of detection for this nanowire (470 nm × 64 nm × 108 nm). The current detection limit of this system is 43 ± 10 molecules.

thermal conductance implies a reduction in the Kapitza length from 55 to 12 nm. These values for the Kapitza lengths are in good agreement with thermal conductance measurements[21] and boundary slip measurements on hydrophobic surfaces.[36] The addition of salt to aqueous solutions interacting with hydrophobic surfaces has been shown to increase the wetting properties of the solution.[37] This suggests that solutes in the water increase the adhesion energy between the aqueous solution and hydrophobic surface. Recently, it has been shown that an increase in adhesion energy,[15,19,20] causes an increase in heat transfer across the interface. This effect is most likely responsible for the observed increase in thermal conductance with increasing solute molality.

An alternative mechanism that could explain the decrease in temperature with increasing solute molality involves elevation of the solvent boiling point with increasing solute molality. This mechanism, involving the colligative properties of water, is attractive because recent results suggests that solar heated nanoparticles in water can be used to generate vapor.[9] Increasing the solute molality will increase the boiling point. If there is vapor surrounding the nanowires then heat transfer to the surrounding liquid will be inhibited and the temperature into the substrate will be increased. When the boiling point is increased, vapor generation is suppressed and heat transferred to the surrounding increased resulting in a lower substrate temperature. We do not believe that this is the mechanism because the range of laser intensity used in our measurements ensured that the local temperature of the nanostructures was below the boiling point of water.

Monitoring the Removal of a Hydrophobic Layer. In order to determine if the thermal conductance is limited by the interface conductance at the gold−liquid interface, a chloroform layer was deposited onto the gold through a sonication bath. The particle is then heated with the laser to displace the hydrophobic chloroform monolayer with water. The temperature was monitored during constant laser excitation of 1.5 × 10^{10} W/m^2. As seen in Figure 4, the local temperature change decreases gradually over time from 295 K until a saturation temperature change of 190 K. The chloroform molecules at the surface are displaced by water molecules with a corresponding change in surface wettability. The interface wettability changes from hydrophobic to hydrophilic. The hydrophilic gold surface dissipates heat more readily than the hydrophobic surface. Because more heat is being dissipated into the surrounding liquid and less into the $Al_{0.94}Ga_{0.06}N$ film the temperature drops. At the saturation temperature, further chloroform displacement does not change the dissipation rate into the liquid and no further temperature change is observed. The local temperature change is converted into a thermal conductance (heat transfer coefficient) using eq 2. The time-dependent thermal conductance is shown as the red dots in Figure 4. The saturation thermal conductance agrees with the interface thermal conductance for a gold hydrophilic surface[21] confirming that the thermal conductance is limited by the interface conductance of the gold liquid interface. As a further check, a 1-dodecanethiol (C_{12}) self-assembled monolayer was adsorbed on a clean sample and a thermal conductance of 50 ± 3 was measured for heat dissipation into water. This value is in agreement with the interface thermal conductance of a 1-octadecanethiol (C_{18}) modified hydrophobic gold surface.[21]

Molecular Sensor Detection Limit. The largest sensitivity to molecular detection is observed when the gold surface is hydrophobic. The interface conductance is smallest under these conditions. This leads to the largest change in slope for temperature change with light intensity with the smallest uncertainty. A change in this slope is easily observed when molecules bind to the surface. In contrast, a hydrophilic surface has the highest thermal conductance where the heat slope is the lowest and is inherently insensitive as a molecular detector. The detection limit where the change in interface conductance due to molecular binding is greater than the three times the standard deviation for pure water thermal conductance is 157 ± 12 sugar molecules (see Figure 7). Interestingly, the smaller thermal conductance for pure water improves the detection limit because the slope of temperature change versus laser intensity is inversely proportional to thermal conductance. The larger slope has the lowest uncertainty in the measurement and the best limit of detection. This detection limit is for a 470 nm long nanowire with an integration time of 0.03 s per pixel. The detection limit can be lowered by increasing the integration time of the measurement and decreasing the size of the nanostructure. A longer integration time reduces the noise by the square root of the integration time and the smaller nanostructure reduces the size of the interface. The interface conductance from the hydrophobic gold nanowires appears to be relatively invariant with size (see Figure 6). Smaller nanostructures, compared to larger nanostructures, have fewer interface molecules and should have a larger proportional change in the interface thermal conductance when displaced by target molecules such as sugar. This scaling law is confirmed by measuring the thermal conductance from 200 and 100 nm long nanowires covered with a 1-dodecanethiol (C_{12}) self-assembled monolayer immersed in pure water and 0.5% by mass solution of D-glucose. This data is shown in the Supporting Information. Also, smaller nanostructures have smaller absorption cross sections. Larger laser intensities can be used on the smaller nanostructure to generate the same change in temperature as larger nanostructures with smaller laser intensities. Larger laser intensity reduces the temperature uncertainties because the counts of Er^{3+} photoluminescence are proportional to laser

dx.doi.org/10.1021/nl401717y | Nano Lett. 2013, 13, 4142−4147

intensity. Presently, the lowest sugar molality that can be detected on the 470 nm nanowire is 0.00193 mol/kg (43 sugar molecules/1.3 × 10^6 water molecules). Increasing the integration time to 1 s should decrease this detection limit to 0.000334 mol/kg and single molecule detection becomes viable from a single nanocylinder, 40 nm diameter and 40 nm high. This size nanodot can be fabricated with e-beam lithography and easily probed with our molecular detection method.

Conclusions. The heat dissipation and thermal conductance from single gold nanowires immersed in aqueous solutions of D-glucose and sodium chloride are examined using a thermal sensor composed of a thin film of $Al_{0.94}Ga_{0.06}N$ with incorporated Er^{3+}. A CW 532 nm laser was used to excite the nanowire and the thermal sensor simultaneously. The measured temperature of the nanowire is a direct function of the thermal conductance at the gold interface. The thermal conductance into the substrate is 82 MW/m^2·K, in agreement with previous measurements. When the sample is immersed in pure water, the thermal conductance into the water is low (~10 MW/m^2·K), indicating a hydrophobic surface interaction with water. The thermal conductance into the aqueous phase increases when solute molecules are bound to the surface. A saturation value of 50 MW/m^2·K is observed. The smallest number of solute molecules attached to the surface giving a measured detectable signal three times the standard deviation of the background signal is 43 ± 10 molecules. This occurs on a nanowire 470 nm long, 108 nm wide, and 64 nm high. Because the thermal conductance does not change with nanostructure size, single molecule detection becomes viable for a single nanocylinder 40 nm in diameter and 40 nm high.

■ ASSOCIATED CONTENT

Ⓢ Supporting Information

The determination of the thermal transfer parameter. This material is available free of charge via the Internet at http://pubs.acs.org.

■ AUTHOR INFORMATION

Corresponding Author

*E-mail: richards@helios.phy.ohiou.edu.

Notes

The authors declare no competing financial interest.

■ ACKNOWLEDGMENTS

The authors thank OSU center of Nanofabrication for their help in fabrication of the nanowires and the Condensed Matter and Surface Science Program at Ohio University.

■ REFERENCES

(1) Bregeon, D.; Colot, V.; Radman, M.; Taddei, F. *Genes Dev.* **2001**, *15* (17), 2295–2306.
(2) Walt, D. R. *Anal. Chem.* **2013**, *85* (3), 1258–1263.
(3) Dickerson, E. B.; Dreaden, E. C.; Huang, X. H.; El-Sayed, I. H.; Chu, H. H.; Pushpanketh, S.; McDonald, J. F.; El-Sayed, M. A. *Cancer Lett.* **2008**, *269* (1), 57–66.
(4) Huang, X. H.; Jain, P. K.; El-Sayed, I. H.; El-Sayed, M. A. *Lasers Med. Sci.* **2008**, *23* (3), 217–228.
(5) Huang, X. H.; Jain, P. K.; El-Sayed, I. H.; El-Sayed, M. A. *Nanomedicine* **2007**, *2* (5), 681–693.
(6) Hirsch, L. R.; Stafford, R. J.; Bankson, J. A.; Sershen, S. R.; Rivera, B.; Price, R. E.; Hazle, J. D.; Halas, N. J.; West, J. L. *Proc. Natl. Acad. Sci. U.S.A.* **2003**, *100* (23), 13549–13554.
(7) Kah, J. C. Y.; Chen, J.; Zubieta, A.; Hamad-Schifferli, K. *ACS Nano* **2012**, *6* (8), 6730–6740.
(8) Wijaya, A.; Schaffer, S. B.; Pallares, I. G.; Hamad-Schifferli, K. *ACS Nano* **2009**, *3* (1), 80–86.
(9) Neumann, O.; Urban, A. S.; Day, J.; Lal, S.; Nordlander, P.; Halas, N. J. *ACS Nano* **2013**, *7* (1), 42–49.
(10) Jiao, P. F.; Zhou, H. Y.; Chen, L. X.; Yan, B. *Curr. Med. Chem.* **2011**, *18* (14), 2086–2102.
(11) Lapotko, D. O.; Lukianova-Hleb, E. Y.; Oraevsky, A. A. *Nanomedicine* **2007**, *2* (2), 241–253.
(12) Dondapati, S. K.; Ludemann, M.; Mueller, R.; Schwieger, S.; Schwemer, A.; Haendel, B.; Kwiatkowski, D.; Djiango, M.; Runge, E.; Klar, T. A. *Nano Lett.* **2012**, *12* (3), 1247–1252.
(13) Kravets, V. G.; Schedin, F.; Jalil, R.; Britnell, L.; Gorbachev, R. V.; Ansell, D.; Thackray, B.; Novoselov, K. S.; Geim, A. K.; Kabashin, A. V.; Grigorenko, A. N. *Nat. Mater.* **2013**, *12* (4), 304–9.
(14) van de Hulst, H. C. *Light Scattering by Small Particles*; John Wiley and Sons, Inc.: New York, 1957.
(15) Losego, M. D.; Grady, M. E.; Sottos, N. R.; Cahill, D. G.; Braun, P. V. *Nat. Mater.* **2012**, *11* (6), 502–506.
(16) Alper, J.; Hamad-Schifferli, K. *Langmuir* **2010**, *26* (6), 3786–3789.
(17) Cicero, G.; Grossman, J. C.; Catellani, A.; Galli, G. *J. Am. Chem. Soc.* **2005**, *127* (18), 6830–6835.
(18) Doshi, D. A.; Watkins, E. B.; Israelachvili, J. N.; Majewski, J. *Proc. Natl. Acad. Sci. U.S.A.* **2005**, *102* (27), 9458–9462.
(19) Shenogina, N.; Godawat, R.; Keblinski, P.; Garde, S. *Phys. Rev. Lett.* **2009**, *102* (15), 156101.
(20) Prasher, R. *Appl. Phys. Lett.* **2009**, *94* (4), 041905.
(21) Ge, Z. B.; Cahill, D. G.; Braun, P. V. *Phys. Rev. Lett.* **2006**, *96* (18), 186101.
(22) Carlson, M. T.; Khan, A.; Richardson, H. H. *Nano Lett.* **2011**, *11* (3), 1061–1069.
(23) Gurumurugan, K.; Chen, H.; Harp, G. R.; Jadwisienczak, W. M.; Lozykowski, H. J. *Appl. Phys. Lett.* **1999**, *74* (20), 3008–3010.
(24) Garter, , M. J.; Steckl, A. J. *IEEE Trans. Electron Devices* **2002**, *49* (1), 48–54.
(25) Carlson, M. T.; Green, A. J.; Richardson, H. H. *Nano Lett.* **2012**, *12* (4), 1534–1537.
(26) Oh, D.-W.; Kim, S.; Rogers, J. A.; Cahill, D. G.; Sinha, S. *Adv. Mater.* **2011**, *23* (43), 5028–5033.
(27) Vernon, K. C.; Funston, A. M.; Novo, C.; Gomez, D. E.; Mulvaney, P.; Davis, T. J. *Nano Lett.* **2010**, *10* (6), 2080–2086.
(28) Ge, Z. B.; Cahill, D. G.; Braun, P. V. *J. Phys. Chem. B* **2004**, *108* (49), 18870–18875.
(29) Despa, F.; Fernandez, A.; Berry, R. S. *Phys. Rev. Lett.* **2004**, *93* (22), 228104.
(30) Russier, V. *Surf. Sci.* **1989**, *214* (1–2), 304–322.
(31) Chao, F.; Costa, M.; Tadjeddine, A. *J. Electroanal. Chem.* **1992**, *329* (1–2), 313–327.
(32) Lum, K.; Chandler, D.; Weeks, J. D. *J. Phys. Chem. B* **1999**, *103* (22), 4570–4577.
(33) Dahlin, A. B.; Zahn, R.; Voeroes, J. *Nanoscale* **2012**, *4* (7), 2339–2351.
(34) Tsionsky, V.; Daikhin, L.; Gileadi, E. *J. Electrochem. Soc.* **1996**, *143* (7), 2240–2245.
(35) Kautek, W.; Sahre, M.; Soares, D. M. *Phys. Chem. Chem. Phys.* **1995**, *99* (4), 667–676.
(36) Cottin-Bizonne, C.; Cross, B.; Steinberger, A.; Charlaix, E. *Phys. Rev. Lett.* **2005**, *94* (5), 056102.
(37) Chaudhuri, R. G.; Paria, S. *J. Colloid Interface Sci.* **2009**, *337* (2), 555–562.